Adaptive Reference Model Predictive Control with Improved Performance for Voltage Source Inverters

Yun Yang, *Student Member,* Siew-Chong Tan, *Senior Member,* Shu Yuen Ron Hui, *Fellow*

***Abstract*—Power converters under the model predictive control (MPC) inherently suffer from non-ignorable steady-state residuals in its control outputs when it exists a mismatch in the parameters between the actual system in control and the system's model adopted in the control. In this paper, an adaptive reference model predictive control (ARMPC) is proposed in response to this issue. Unlike those conventional derivatives of MPC, the ARMPC is designed to track the so-called virtual references instead of the actual references. The virtual references are generated by a flexibly modeled virtual multiple input multiple output (MIMO) system. Consequently, additional tuning is not required for different operating conditions. ARMPC has been applied to a single-phase full-bridge voltage source inverter (VSI) with both resistive and resistive-inductive (*RL*) loads. It is experimentally verified that the proposed ARMPC can significantly attenuate the steady-state offsets in the environment of model mismatch (which is an inherent problem of MPC without significantly sacrifice transient performance). Also, a demonstration that ARMPC renders a consistent attenuation of steady-state errors than the conventional MPC with integrator is provided. More importantly, ARMPC shows better transient performance than the MPC with integrator for some cases.**

***Index Terms*—Adaptive reference model predictive control (ARMPC), model predictive control (MPC), virtual references, virtual MIMO system, MPC with integrator.**

I. Introduction

THE technology of power converters has gone through rapid advancement during the last five decades and its applications are fast expanding, ranging from industrial to residential applications [1], [2]. Power electronics circuits are nonlinear systems with hybrid nature, including linear and nonlinear parts and a finite number of switching devices. To achieve power regulations, hysteresis control and linear control with pulse width modulation (PWM) based on the analog circuits have been widely used for decades [3]. However, with the development of faster, cheaper, and more powerful microprocessors, the implementation of new and more complex control schemes is possible.

Model predictive control (MPC) is a type of optimal control strategy based on numerical optimization. It is a process control strategy in which the future control inputs and system response are predicted using a system model and optimized at regular intervals with respect to a performance index [4]–[6], which appears to be a possible alternative for the control of power electronics [7]–[10]. MPC includes a wide family of controllers [5], [11], [12]. In particular, one of the most attractive predictive strategies for power electronics is the finite-control-set model predictive control (FCS-MPC) [7]–[10]. Unlike the conventional MPC, the calculation of the optimal actuation of FCS-MPC is achieved through the online evaluation of the finite number of switching states in the system, which requires no modulator. FCS-MPC inherits several advantages. First, the concept of FCS-MPC is intuitive. Second, the criteria of FCS-MPC to minimize the cost function are quite flexible and easily programmable. Third, FCS-MPC provides a systematic method of dealing with constraints on inputs and states, which is important for the control of complex power electronic systems with multiple variables. Besides, FCS-MPC can improve the operation of the system by only including restrictions on some variables.

An eligible FCS-MPC requires the actual system model. Practically, most predictive models are derived from the nominal model of the system that expresses the circuit in terms of a fixed set of components and parameters specified in the design, which may deviate from the actual system model. Furthermore, the nominal model is typically a simplified approximated model of the actual system as precise description of the actual system model in state-space form is typically impossible. Besides, power electronic systems may own varying parameter values that change with temperature, operating conditions, and operating timespan. They are susceptible to external disturbance. All these possible scenarios lead to a parametric mismatch in the model between the actual power electronic system and the predictive system, which could result in the existence of steady-state errors for the actual system [10]. To overcome such steady-state errors, several schemes have been proposed [7]–[9]. In [7], MPC with Kalman filter is proposed to deal with unmeasured load variations and to attenuating the steady-state offsets. In [8], an adaptive robust predictive current control removes the current error by operating the control in parallel with the deadbeat algorithm. In [9], the proposed MPC with integrator reduces the steady-state errors at the sampling instant and during the intersampling. This paper presents an adaptive reference model predictive control (ARMPC) that integrates the merits of the strategies in [7]–[9] and incorporates trajectory-based control [13]–[21]. It is an extended version of [22]. To further validate the utility of ARMPC to alleviate the steady-state errors of power converters for different cases and stress the merits of the dynamic performance, a comprehensive presentation of ARMPC is provided in this paper.

ARMPC consists of two major units, virtual reference and virtual multiple input multiple output (MIMO) system. Instead of tracking the actual references for the conventional MPC,

Manuscript received January 20, 2016; revised April 21, 2016, June 30, 2016, October 05, 2016; accepted February 11, 2016. This work is supported by the Hong Kong Research Grant Council under Theme-based Research Project: T23-701/14-N. Recommended by Associate Editor A. Chakrabortty.

Y. Yang and S. C. Tan are with the Department of Electrical and Electronic Engineering, The University of Hong Kong, Hong Kong (e-mail: yangyun@eee.hku.hk, sctan@eee.hku.hk).

S. Y. R. Hui is with the Department of Electrical and Electronic Engineering, The University of Hong Kong, Hong Kong and also with the Department of Electrical and Electronic Engineering, Imperial College London, London SW7 2AZ, U.K. (e-mail: ronhui@eee.hku.hk).

virtual references are used for the predictive strategy in ARMPC. Virtual MIMO system derives the virtual references as outputs that are based on the trajectories in the states plane, which can be flexibly modeled. According to the severity of the model mismatch, the complexity and accuracy of the algorithm for the virtual MIMO system are selected appropriately. The advantages of ARMPC over the derivatives of the conventional MPC, including MPC with Kalman filter, adaptive robust predictive current control, and MPC with integrator, are simple algorithm, easy implementation in low-price micro-controllers, less tuning, and inferior steady-state performance [22].

In this paper, ARMPC is applied to a single-phase full-bridge VSI with both resistive and resistive-inductive (*RL*) load. It is experimentally verified that ARMPC owns better steady-state performance than the conventional MPC and MPC with integrator. The comparisons of ARMPC, MPC, and MPC with integrator in transient are also provided. Despite the illustration of the adoption of ARMPC in this paper is only on the VSI, the proposed ARMPC has potential to be widely applied to other power electronics devices.

II. Steady-State Errors of Existing MPC Systems

Consider a discrete linear time-invariant power electronics system with disturbance [23]

$$\begin{cases} \mathbf{x}(k+1) = \mathbf{A}\mathbf{x}(k) + \mathbf{B}\mathbf{u}(k) + \mathbf{B_d}\mathbf{d}(k) \\ \mathbf{y}(k) = \mathbf{C}\mathbf{x}(k) + \mathbf{C_d}\mathbf{d}(k) \\ \mathbf{u}(k) \in P := \{u_1, u_2, \ldots, u_p\} \end{cases}, \tag{1}$$

Where $\mathbf{x}(k) \in \mathbb{R}^n$ denotes the vector of discrete-time state variable; $\mathbf{y}(k) \in \mathbb{R}^m$ is the output vector; $\mathbf{u}(k)$ is the switching signal; $\mathbf{d}(k) \in \mathbb{R}^d$ is the constant disturbance vector, i.e., $\mathbf{d}(k+1) = \mathbf{d}(k)$; $\mathbf{A} \in \mathbb{R}^{n\times n}$, $\mathbf{B} \in \mathbb{R}^{n\times p}$, $\mathbf{C} \in \mathbb{R}^{m\times n}$, $\mathbf{B_d} \in \mathbb{R}^{n\times d}$, $\mathbf{C_d} \in \mathbb{R}^{m\times d}$, ($\mathbf{A}$, $\mathbf{B}$) is controllable and ($\mathbf{C}$, $\mathbf{A}$) is observable. p is the number of modes of the switched power electronics system. The objective is to design an MPC controller based on a linear system model to have the output $\mathbf{y}(k)$ track the reference $\mathbf{y_r}(k)$, where $\mathbf{y_r}(k) \in \mathbb{R}^m$ is an asymptotically constant reference vector.

However, a simplified linear model for the MPC design as

$$\begin{cases} \mathbf{x}(k+1) = \mathbf{A}\mathbf{x}(k) + \mathbf{B}\mathbf{u}(k) \\ \mathbf{y}(k) = \mathbf{C}\mathbf{x}(k) \end{cases} \tag{2}$$

is generally adopted as the predicted equation, which derives

$$\begin{bmatrix} \mathbf{A}-\mathbf{zI} & \mathbf{B} \\ \mathbf{C} & \mathbf{O} \end{bmatrix} \begin{bmatrix} \hat{\mathbf{x}}(k) \\ \mathbf{u}(k) \end{bmatrix} = \begin{bmatrix} \mathbf{O} \\ \mathbf{y}(k) \end{bmatrix}, \tag{3}$$

where $\hat{\mathbf{x}}(k)$ is the predicted states; $\mathbf{I}$ is an n-dimensional unity matrix, $\mathbf{O}$ is a null matrix, and $\mathbf{z}$ is the Z-transform variable. An ideal controller is required for the output of the system to track the reference such that

$$\begin{bmatrix} \mathbf{A}-\mathbf{zI} & \mathbf{B} \\ \mathbf{C} & \mathbf{O} \end{bmatrix} \begin{bmatrix} \mathbf{x}(k) \\ \mathbf{u_c}(k) \end{bmatrix} = \begin{bmatrix} -\mathbf{B_d}\mathbf{d}(k) \\ \mathbf{y_r}(k) - \mathbf{C_d}\mathbf{d}(k) \end{bmatrix}, \tag{4}$$

where $\mathbf{u_c}(k)$ is the desired control signal.

Then, it is defined that $\Delta\mathbf{x}(k) = \hat{\mathbf{x}}(k) - \mathbf{x}(k)$, $\Delta\mathbf{u}(k) = \mathbf{u}(k) - \mathbf{u_c}(k)$ and the offset $\boldsymbol{\delta}(k) = \mathbf{y}(k) - \mathbf{y_r}(k)$. By subtracting (3) and (4),

$$\begin{bmatrix} \mathbf{A}-\mathbf{zI} & \mathbf{B} \\ \mathbf{C} & \mathbf{O} \end{bmatrix} \begin{bmatrix} \Delta\mathbf{x}(k) \\ \Delta\mathbf{u}(k) \end{bmatrix} = \begin{bmatrix} \mathbf{B_d}\mathbf{d}(k) \\ \boldsymbol{\delta}(k) + \mathbf{C_d}\mathbf{d}(k) \end{bmatrix} \tag{5}$$

can be obtained.

Based on (5), we can derive

$$\boldsymbol{\delta}(k) = \mathbf{C}\Delta\mathbf{x}(k) - \mathbf{C_d}\mathbf{d}(k). \tag{6}$$

Apparently, $\boldsymbol{\delta}(k) \neq \mathbf{0}$, which denotes the existence of steady-state errors when the conventional MPC is adopted to regulate a power electronics system.

The single-phase full-bridge VSI is a very well-known power electronics device that can be used as an AC source or in applications such as the uninterruptable power supply (UPS), active filter, and grid-tied inverter, etc. [2]. Most previous works on VSI that is controlled by MPC are limited to current control and the load is an *RL* load [24]–[27]. Even though the voltage control version of MPC is studied in [28], it is noted that a current observer is still needed. However, in many applications, it is necessary to control the output voltage to directly follow a reference and an *LC* filter is installed between the bridge and the *RL* load, as illustrated in Fig. 1. This makes the use of predictive current control cumbersome since a cascaded structure or look-up table for deriving the voltage reference will be required. Therefore, MPC that is based on voltage control is typically more applicable for VSI with an *LC* filter.

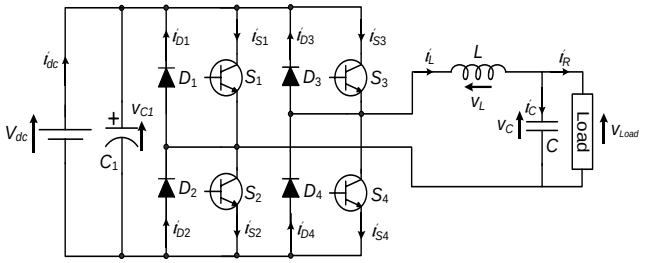

Fig. 1. Single-phase full-bridge VSI with *LC* filter.

The discrete model of the VSI with purely resistive load is provided in [22]. The discrete model of the VSI with *RL* load using Euler's forward method is

$$\begin{cases} v_C(k+1) = v_C(k) + \dfrac{T_s}{C} i_L(k) - \dfrac{T_s}{C} i_R(k) \\ i_L(k+1) = -\dfrac{T_s}{L} v_C(k) + i_L(k) + \dfrac{V_{dc} T_s}{L} i_R(k), \\ i_R(k+1) = \dfrac{T_s}{L_1} v_C(k) + \left(1 - \dfrac{RT_s}{L_1}\right) i_R(k) \end{cases} \tag{7}$$

where T_s is the sampling time; L_1 and R are the inductance and resistance of the load, respectively. Note that with the fast computational capability of emerging controller hardware (e.g. DSP TMS320F28069 with a 32-Bit CPU of 90 MHz) and the

system's order of the VSI with an *RL* load being only three, the discretization introduces very small quantization errors [10].

By adopting the two-step ahead prediction for compensating the calculation delay of the MPC [29], the predicted voltage at the sampling time k+1 will be used for the optimization based on the measurements of $v_C(k-1)$, $i_L(k-1)$, $i_R(k-1)$, and the applied control input $u(k-1)$, which is given as

$$\hat{v}_C(k+1)=\left(1-\frac{T_s^2}{LC}-\frac{T_s^2}{L_1C}\right)v_C(k-1)+\frac{2T_s}{C}i_L(k-1)+\left(\frac{RT_s^2}{L_1C}-\frac{2T_s}{C}\right)i_R(k-1)+\frac{V_{dc}T_s^2}{LC}u(k-1). \quad (8)$$

The cost function is designed to contain two terms. One is called the primary term, which is established in order to provide a proper system behavior. The primary term is expressed in a general way as the error between the reference voltage and the predicted voltage at the sampling time k+1, as derived in (8). The other is named the secondary term, which is established to improve system's performance. The secondary term is expressed as the number of switching actions taken from sampling time k−1 to sampling time k and the objective of the cost function is to minimize the required switching frequency so as to improve the converter's efficiency. The expression of the cost function is

$$J=\Gamma_y\left[v_{\text{ref}}(k+1)-\hat{v}_C(k+1)\right]^2+\Gamma_u\left[u(k)-u(k-1)\right]^2, \quad (9)$$

where $v_{\text{ref}}(k+1)$ is the actual reference at the sampling time k+1. Γ_y and Γ_u are the weighting factors.

Then, the trajectory for tracking the reference can be found by solving

$$u^*(k)=\arg\min_{u\in\{-1,0,1\}} J. \quad (10)$$

Unlike those traditional optimization solvers for quadratic programming (QP) problems, such as the active set method and the interior point method, the decision making of (10) is algorithmic. In particular, in the period of the sampling time k−1 and k, three possible control input values are substituted in (10) to check which control input gives the minimum value of the objective function. The selected input is named as the optimal control signal at the sampling time k from all the possible control inputs of u = −1, 0 and 1, which is denoted as $u^*(k)$. The corresponding control diagram can be depicted as shown in Fig. 2.

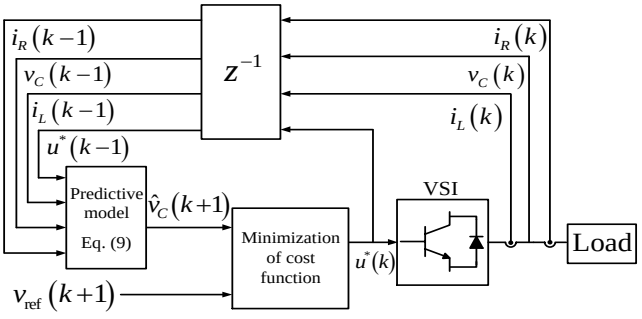

Fig. 2. Control block diagram of MPC for VSI with *RL* load.

In trajectory-based control theory, the natural trajectories of a system will be corresponding to the actual state-space model of that system [13]. If there exists model mismatch, the natural trajectories of the system will be changed, which is illustrated by the simulation results of VSI with purely resistive load in [22]. In this paper, simulation results of the state trajectory (for state i_L and v_C) and the corresponding output voltage of the VSI with *RL* load are given in Fig. 3, which presents the state trajectory and the corresponding output voltage before and after the appearance of model mismatch.

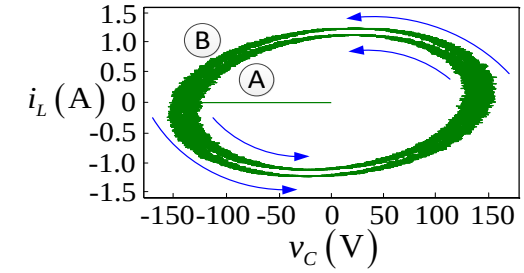

(a) State trajectory

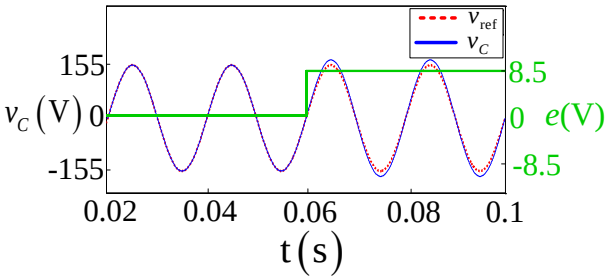

(b) Corresponding output voltage

Fig. 3. State trajectory and the corresponding output voltage of VSI with *RL* load before and after the appearance of model mismatch.

In Fig. 3(a), when the system is introduced a model mismatch, the state trajectory changes from circle *A* to circle *B*. Fig. 3(b) shows the output voltage is incapable of tracking the reference accurately, i.e., the difference of the root-mean-square (RMS) value between the reference and the output voltage is increased from 0 V to 8.5 V.

III. Proposed ARMPC for Power Electronics

Consider that the reference $\mathbf{y_r}(k)$ in (4) is replaced by the virtual reference $\mathbf{y'_r}(k)$ as

$$\begin{bmatrix}\mathbf{A}-\mathbf{zI} & \mathbf{B}\\ \mathbf{C} & \mathbf{O}\end{bmatrix}\begin{bmatrix}\mathbf{x}(k)\\ \mathbf{u_c}(k)\end{bmatrix}=\begin{bmatrix}-\mathbf{B_d}\mathbf{d}(k)\\ \mathbf{y'_r}(k)-\mathbf{C_d}\mathbf{d}(k)\end{bmatrix}. \quad (11)$$

We define $\boldsymbol{\delta}'(k)=\mathbf{y_r}(k)-\mathbf{y'_r}(k)$. By subtracting (3) and (11), we obtain

$$\begin{bmatrix}\mathbf{A}-\mathbf{zI} & \mathbf{B}\\ \mathbf{C} & \mathbf{O}\end{bmatrix}\begin{bmatrix}\boldsymbol{\Delta}\mathbf{x}(k)\\ \boldsymbol{\Delta}\mathbf{u}(k)\end{bmatrix}=\begin{bmatrix}\mathbf{B_d}\mathbf{d}(k)\\ \boldsymbol{\delta}(k)+\boldsymbol{\delta}'(k)+\mathbf{C_d}\mathbf{d}(k)\end{bmatrix}. \quad (12)$$

Apparently, if the virtual references $\mathbf{y'_r}(k)$ are designed properly, such that

$$\boldsymbol{\delta}'(k)=\mathbf{C}\boldsymbol{\Delta}\mathbf{x}(k)-\mathbf{C_d}\mathbf{d}(k) \quad (13)$$

is satisfied, $\boldsymbol{\delta}(k) = \mathbf{0}$, which means the offsets can be theoretically eliminated.

Similar to the geometric interpretation of virtual references for the operation of VSI in [22], an illustration of a general power electronics system (1) is shown in Fig. 4 to present the role of virtual references in reducing the steady-state errors. To explicitly exhibit advantages of using virtual references in a plane, only one output element y_1 of the output vector $\mathbf{y}$ is considered in Fig. 4. Apparently, the output chosen by MPC (which is depicted as red lines) will lead to offsets after the appearance of model mismatch. However, if the output is made to track the virtual references, which is plotted in orange dot lines instead of the actual reference, the steady-state errors in the system controlled by MPC can be decreased.

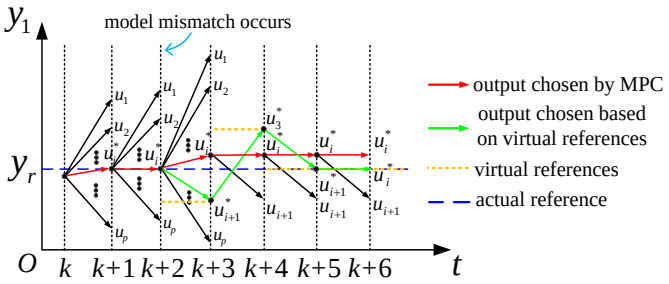

Fig. 4. Outputs of the system with model mismatch and virtual references.

Then, developing a virtual MIMO system from the basis of trajectory-based control [13]–[21] to generate the virtual references is critical for the design of ARMPC. The modeling of virtual MIMO system can be diversified, but is highly affected by the specific characteristics of the objective system. In [22], a linear fitting method is adopted for virtual MIMO system considering the scale of the model mismatch of VSI in the experiments. In this paper, inheriting the simplicity and utility of the virtual MIMO system in [22], more stringent descriptions of the proposed virtual MIMO system with boundary settings are provided. In this work on VSI, however, it is only necessary to use a virtual multiple input single output (MISO) system to accomplish the function of generating the required virtual references. Nevertheless, for the sake of generality, the term virtual MIMO system will be adopted hereinafter as a common terminology for systems adopting this approach. A geometric illustration of the virtual MIMO system for the VSI studied in this paper can be plotted in Fig. 5. To reduce the steady-state errors between the operating trajectory and the actual reference trajectory, the virtual reference trajectory outside the actual reference trajectory is tracked, such that the operating trajectory can be located to operate on the actual reference trajectory. A converse case that the operating trajectory is located outside the actual reference trajectory can be found in [22]. Both cases exhibit the function of virtual MIMO system to make the consistency of the operating trajectory and the actual reference trajectory.

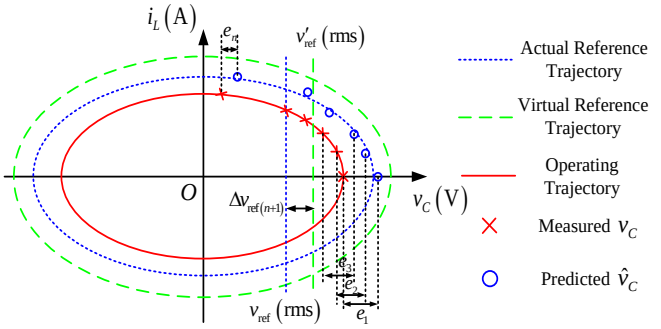

Fig. 5. Modeling of virtual MIMO system in the state plane for the VSI.

The implementation of the virtual MIMO system is based on several past data including states of the state variables and virtual references. For example, the error between the predicted output voltage $\hat{v}_C(k)$ derived by the predicted control law (8) based on the stored data of $v_C(k-2)$, $i_L(k-2)$, $u(k-2)$, and the measured output voltage $v_C(k)$ is defined as

$$e(k) = \hat{v}_C(k) - v_C(k). \tag{14}$$

Then, $2n$ past data of the errors

$$\mathbf{e} = \begin{bmatrix} e(k-2n+1) & e(k-2n+2) & \dots & e(k) \end{bmatrix} \tag{15}$$

are stored and used for the virtual MIMO system. In the meantime, the variation of virtual references for the last n sampling is

$$\Delta\mathbf{v}_{\text{ref}} = \begin{bmatrix} \Delta v_{\text{ref}}(k-n+1) & \Delta v_{\text{ref}}(k-n+2) & \dots & \Delta v_{\text{ref}}(k) \end{bmatrix}. \tag{16}$$

Since linear fitting method is adopted for the modeling of the virtual MIMO system, the mathematical expression of the virtual MIMO system is

$$\Delta\mathbf{v}_{\text{ref}}^{\text{T}} = \begin{bmatrix} e(k-2n+1) & e(k-2n+2) & \cdots & e(k-n) \\ e(k-2n+2) & e(k-2n+3) & \cdots & e(k-n+1) \\ \vdots & \vdots & \ddots & \vdots \\ e(k-n) & e(k-n+1) & \cdots & e(k-1) \end{bmatrix} \mathbf{K}^{\text{T}}, \tag{17}$$

where $\mathbf{K} = [K_1 \quad K_2 \quad \dots \quad K_n]$ represents the weighting factors of the errors on the variation of virtual references. The error matrix is nonsingular, because discretization via Euler's forward method introduces nonzero errors between the predicted output voltage $\hat{v}_C$ and the measured output voltage v_C even if the system is free of model mismatch. For the system with model mismatch, the errors in the matrix can be larger, because the disturbance factor has not been included in (8). Besides, since the sampling frequency of the controllers used in power electronics is much higher than the frequency of v_C [13]. As shown in Fig. 6, from $e(k-2n+1)$ to $e(k-1)$, the errors are in the same period of v_C, such that

$$\frac{e(k-n)}{e(k-2n+1)} \neq \frac{e(k-n+1)}{e(k-2n+2)} \neq \cdots \neq \frac{e(k-1)}{e(k-n)}. \tag{18}$$

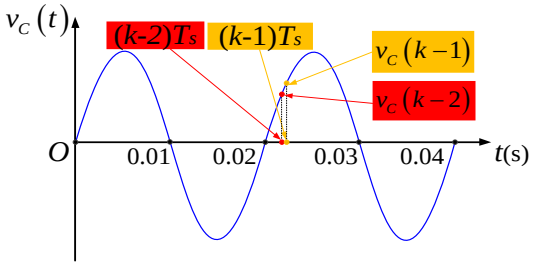

(a) Output voltage v_C

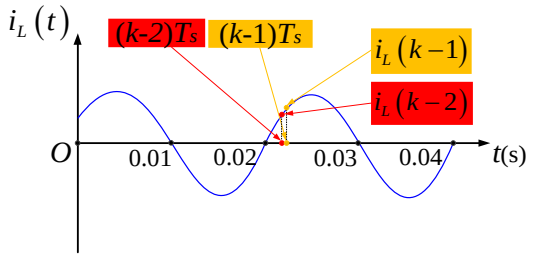

(b) Inductor current i_L

Fig. 6. Two adjacent samples of v_C and i_L of the VSI.

Because of (18), the columns of the error matrix are linearly independent. Therefore, the error matrix can be considered nonsingular. Then, **K** can be derived from (17) as

$$\mathbf{K}=\Delta\mathbf{v}_{\mathrm{ref}}\left(\begin{bmatrix} e(k-2n+1) & e(k-2n+2) & \cdots & e(k-n) \\ e(k-2n+2) & e(k-2n+3) & \cdots & e(k-n+1) \\ \vdots & \vdots & \ddots & \vdots \\ e(k-n) & e(k-n+1) & \cdots & e(k-1) \end{bmatrix}^{-1}\right)^{\mathrm{T}}. \quad (19)$$

By multiplying the derived matrix **K** in (19) and $[e(k-n+1) \quad e(k-n+2) \quad \ldots \quad e(k)]^{\mathrm{T}}$, the variation of the virtual reference $\Delta v_{\mathrm{ref}}(k+1)$ can be obtained as

$$\Delta v_{\mathrm{ref}}(k+1)=\mathbf{K}\left[e(k-n+1) \quad e(k-n+2) \quad \ldots \quad e(k)\right]^{\mathrm{T}}. \quad (20)$$

Then, the first row of the error matrix $[e(k-2n+1) \quad e(k-2n+2) \quad \ldots \quad e(k-n)]$ and $\Delta v_{\mathrm{ref}}(k-2n+1)$ in the vector $\Delta\mathbf{v}_{\mathrm{ref}}$ in (19) are replaced by $[e(k-n+1) \quad e(k-n+2) \quad \ldots \quad e(k)]$ and $\Delta v_{\mathrm{ref}}(k+1)$ respectively to derive a new **K** for the next iteration. The whole process detect the information of model mismatch of VSI instantly and generate variation of the virtual references simultaneously.

The objective function of ARMPC for VSI with *RL* load is

$$J=\Gamma_y\left[\hat{v}_{\mathrm{ref}}(k+1)-\hat{v}_C(k+1)\right]^2+\Gamma_u\left[u(k)-u(k-1)\right]^2, \quad (21)$$

where $\hat{v}_{\mathrm{ref}}(k+1)$ is the virtual reference and

$$\hat{v}_{\mathrm{ref}}(k+1)=\hat{v}_{\mathrm{ref}}(k)+\Delta v_{\mathrm{ref}}(k). \quad (22)$$

The flowchart of the algorithm of ARMPC for the VSI with *RL* load is shown in Fig. 7. The optimization process of ARMPC is the same as the optimization process in (10). To guarantee the stability of the controlled VSI, the boundaries for the virtual references are set within a feasible zone for a heuristic stability assurance. Virtual references of ARMPC are required to be located within the feasible zone. If the virtual reference is outside this zone, which corresponds to the RMS value of v_c being larger than v_{HB}(rms) or smaller than v_{LB}(rms), the virtual reference will be set to v_{HB}(rms) and v_{LB}(rms), respectively. This boundary setting of virtual references ensures that the state variables are within their acceptable ranges which keep the VSI system working stably. A 10% tolerance for the output voltage is set in the experiment, which is validated by numerous tests.

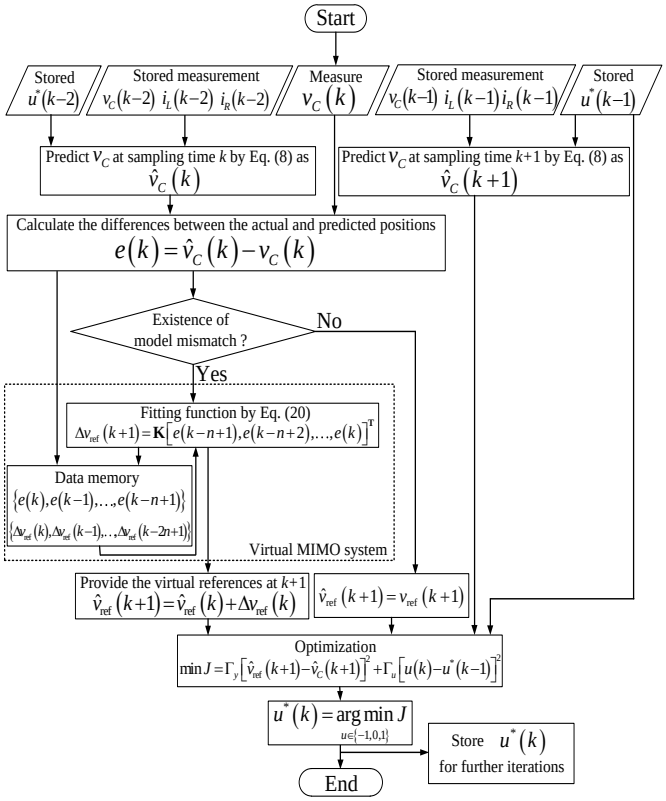

Fig. 7. Flowchart of ARMPC for the VSI with RL load.

IV. Experimental Verification

The experiment is conducted on a Texas Instruments' C2000™ Solar DC/AC single phase inverter [30]. The DSP used for the control is TI's F28069 Piccolo controlCARD. The DC power supply is the programmable source CSW5550 from California Instruments. The purely resistive load used are three incandescent bulbs, at nominal power of 20 W and nominal voltage of 110 V. In the nominal model of the VSI system adopted in this experiment, the bulbs are connected in parallel as the nominal load. The *RL* load used are Kikusui's electronic load PLZ303WH in series with a 0.249 H inductor. The nominal DC input voltage of VSI with both resistive and *RL* load V_{dc} is 165 V. The reference of VSI with both resistive and *RL* load v_{ref} in RMS is 110 V. The specifications of the VSI are given in Table I. Detailed values of the components can be found in the datasheets [30]. The number of the restored data $\Delta\mathbf{v}_{\mathrm{ref}}$ for the virtual MIMO system is 3. The lower bound of the virtual reference v_{LB}(rms) is set at 100 V and the upper bound of the virtual reference v_{HB}(rms) is set at 120 V based on numerous tests under satisfied tolerances. After comparisons,

TABLE II. COMPARISONS OF v_C(RMS) BETWEEN MPC, MPC WITH INTEGRATOR AND ARMPC

Case	MPC	Error	MPC with integrator	Error	ARMPC	Error
Nominal model	106.001 V	**3.64%**	110.020 V	**0.02%**	110.042 V	**0.04%**
Tuned model	110.040 V	**0.04%**	109.832 V	**0.15%**	110.040 V	**0.04%**
One bulb is out (tuned model)	112.511 V	**2.28%**	108.843 V	**1.05%**	110.059 V	**0.05%**
Two bulbs are out (tuned model)	113.091 V	**2.81%**	108.159 V	**1.67%**	110.060 V	**0.05%**
One bulb is out (nominal model)	107.940 V	**1.87%**	109.170 V	**0.08%**	110.081 V	**0.07%**
Two bulbs are out (nominal model)	108.031 V	**1.79%**	108.933 V	**0.10%**	109.995 V	**0.00%**
V_{dc} is changed to 173 V (tuned model)	110.122 V	**0.11%**	109.994 V	**0.00%**	110.011 V	**0.01%**
V_{dc} is changed to 180 V (tuned model)	111.611 V	**1.46%**	110.020 V	**0.02%**	110.058 V	**0.05%**
V_{dc} is changed to 188 V (tuned model)	112.114 V	**1.92%**	110.041 V	**0.04%**	110.040 V	**0.04%**
V_{dc} is changed to 195 V (tuned model)	112.707 V	**2.46%**	110.043 V	**0.04%**	110.002 V	**0.00%**
V_{dc} is changed to 173 V (nominal model)	107.251 V	**2.50%**	109.980 V	**0.02%**	109.963 V	**0.04%**
V_{dc} is changed to 180 V (nominal model)	107.882 V	**1.93%**	110.019 V	**0.02%**	110.023 V	**0.02%**
V_{dc} is changed to 188 V (nominal model)	108.361 V	**1.49%**	110.041 V	**0.04%**	110.020 V	**0.02%**
V_{dc} is changed to 195 V (nominal model)	108.922 V	**0.98%**	110.091 V	**0.08%**	110.057 V	**0.05%**
Average of the relative error		**1.81%**		**0.24%**		**0.03%**

TABLE I. SPECIFICATIONS OF THE NOMINAL VSI

Description	Parameter	Value
Input capacitor	C_1	470 μF
IGBT switches (including parasitic diodes)	S_1, S_2, S_3, S_4 D_1,D_2,D_3,D_4	IRG4PC30FDPBf
Inductance of output filter	L	7 mH
Capacitance of output filter	C	1 μF
Rated input voltage	V_{dc}	165 V
Output voltage reference	v_{ref}	110 V

the weighting factors are set as Γ_y=0.9 and Γ_u=0.1. The switching frequency of VSI in all the scenarios in the experiment is set as 20 kHz. The Keysight's 34401A Multimeter is used to measure the values of v_C for all the cases in this paper. In addition, it is emphasized that the errors of the error matrix in the experiment are bigger than the theoretical ones (because of unavoidable hardware delays and calculation errors of the digital controller), which is verified in experiment.

A. Results of VSI with Resistive Load

1) Steady-State Performance

Comprehensive comparisons of the conventional MPC, MPC with integrator, and ARMPC being applied to the VSI with resistive load for the case of load variation and input voltage V_{dc} fluctuation are provided in [22]. In summary, the comparative results can be concluded in Table II.

Here, the nominal model is the predictive model of using the parametric values provided by the TI's datasheet. In reality, model mismatch exists between the nominal model and the actual VSI with resistive load. If the nominal model is adopted for the MPC, steady-state errors will exist. Tuned model is a near optimal predictive model that the steady-state offsets of the practical inverter is minimal even when the conventional MPC is adopted (negligible steady-state errors exist due to quantization error of DSP). It is possible to fine-tune the coefficients of $v_C(k-1)$ by trial-and-error to obtain a tuned model for the control since precise model of the actual VSI with resistive load is unavailable. It is experimentally found via numerous tests that the steady-state performance of the system is highly sensitive to the coefficients of $v_C(k-1)$ but is insensitive to the coefficients of $i_L(k-1)$ and $u(k-1)$. Hence, both the coefficients of $i_L(k-1)$ and $u(k-1)$ are kept unchanged in the predicted equation for MPC. The measurements show that MPC with the tuned model has an excellent regulation performance and the RMS value of v_C is about 110.04 V at steady state, which is about 0.04% deviation from the reference. MPC with integrator proposed in [9] is also adopted with a proper tuning of K_i=0.25. By using MPC with integrator, the steady-state residual is reduced to 0.02% for the nominal model. Comparisons of relative errors of the output voltage between MPC, MPC with integrator and ARMPC when load and input voltage change in Table II mainly shows two major advantages of ARMPC over MPC and MPC with integrator:

1. ARMPC can significantly reduce the steady-state errors of VSI with resistive load when different types of model mismatch occurs as compared to the conventional MPC.
2. ARMPC can be considered as an "auto-tuning" MPC with integrator, which extensively reduces the steady-state residuals over a wider operating range as compared to the MPC with integrator.

2) Dynamic Performance

Several tests on load and input voltage changes have been conducted. Fig. 8 shows the transient performance of the VSI controlled by MPC, MPC with integrator and ARMPC based on the tuned model when the load changes from three bulbs to two bulbs. Compared with MPC (settling time of 0.8 ms), both MPC with integrator (setting time of 1.2 ms) and ARMPC (settling time of 1.3 ms) have slightly longer duration of transient.

Same conclusion can also be drawn when the load changes from three bulbs to one bulb. The transient period of VSI controlled by both ARMPC and MPC with integrator based on the tuned model are 1.2 ms, only slightly longer than the transient period of 1.0 ms of MPC when the loads changes from three bulbs to one bulb. Then, experiments are carried out for the input voltage changing from 165 V to 180 V and 165 V to 195 V, respectively. When the input voltage is changed from

165 V to 180 V, v_C of VSI controlled by MPC based on the tuned model can instantaneously reach the steady state. Meanwhile, v_C of VSI controlled by ARMPC based on the tuned model takes about 0.6 ms to settle to the steady state. Besides, v_C of VSI controlled by MPC with integrator based on the tuned model having a transient settling time of 1.2 ms.

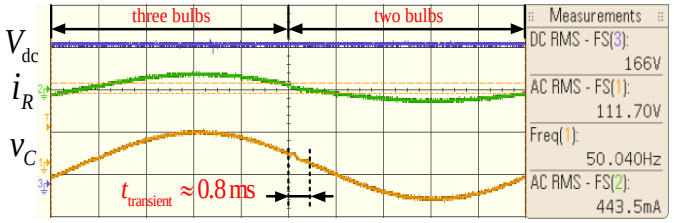

(a) MPC

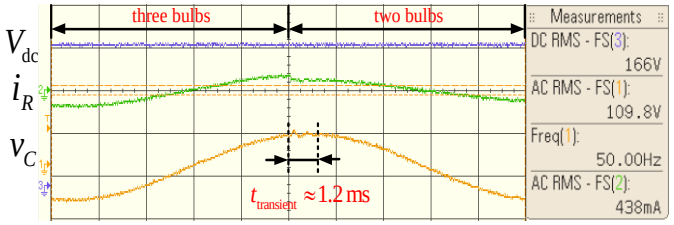

(b) MPC with integrator

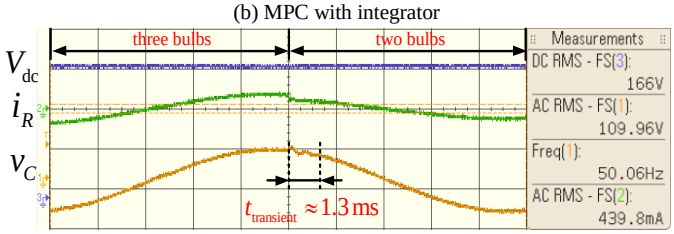

(c) ARMPC

Fig. 8. Transient performance of VSI with load change (three bulbs to two bulbs) controlled by (a) MPC, (b) MPC with integrator and (c) ARMPC based on the tuned model.

Obviously, ARMPC takes only a little longer time to the steady state than MPC and the transient duration is about half of that of MPC with integrator. The same conclusion can also be drawn from the results of the case that the input voltage is changed from 165 V to 195 V. An explicit comparison of the transient period for the four cases among MPC, ARMPC, and MPC with integrator via bar-charts are depicted in Fig. 9.

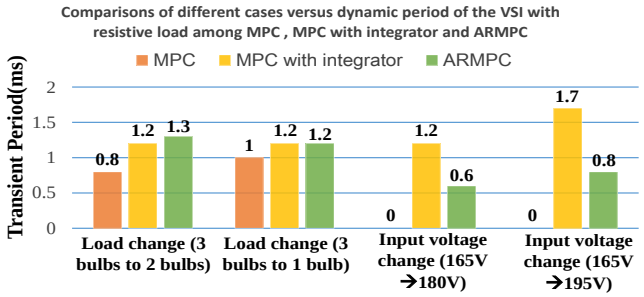

Fig. 9. Comparative bar-charts of different cases versus transient period between the VSI with resistive load controlled by MPC, MPC with integrator, and ARMPC based on the tuned model.

B. *Results of VSI with RL Load*

1) Steady-State Performance

The aforementioned two advantages of ARMPC over MPC and MPC with integrator are also experimentally verified on the VSI with an *RL* load. All three controllers are initially applied based on the nominal model that: input voltage V_{dc}=165 V, reference v_{ref} =110 V and R=100 Ω, L=0.249 H. For MPC, the experimental results shows that the output voltage is 104.291 V at steady state, which is 5.42% deviation from the reference. For MPC with integrator, the output voltage is 109.549 V at steady state, which is 0.41% deviation from the reference. For ARMPC, the output voltage is 109.637 V at steady state, which is 0.33% deviation from the reference. Then, the input voltage V_{dc} changes from 173 V to 180 V to 188 V to 195 V and the comparisons of relative error among MPC, MPC with integrator and ARMPC for different V_{dc} is provided in Fig. 10. Obviously, VSI with *RL* load being controlled by MPC with integrator and ARMPC have better steady-state performance than VSI with *RL* load being controlled by MPC.

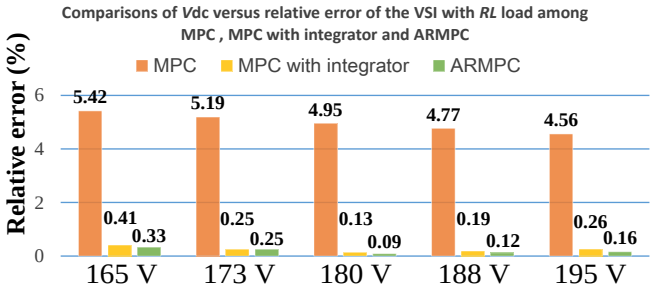

Fig. 10. Comparative bar-charts of V_{dc} versus relative error of v_C between the VSI with *RL* load controlled by MPC, MPC with integrator and ARMPC based on the nominal model.

Next, the experiments are performed on the VSI with *RL* load based on the change of resistance of the load in order to observe the load effect on the output performance. The resistance of the *RL* load changes from 80 Ω to 90 Ω to 100 Ω to 110 Ω to 120 Ω. The corresponding relative errors of v_C of the VSI with *RL* load being regulated by MPC, MPC with integrator and ARMPC are shown in Fig. 11. Both MPC with integrator and ARMPC can significantly reduce the steady-state residuals. Besides, ARMPC can tolerate a wider range of load deviations than the MPC with integrator without tunings for the coefficients like the K_i of the MPC with integrator.

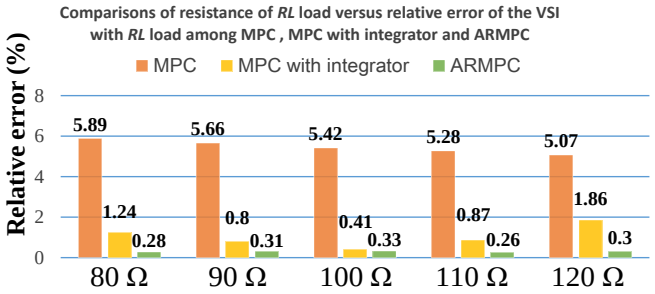

Fig. 11. Comparative bar-charts of resistance of *RL* load versus relative error of v_C between the VSI with *RL* load controlled by MPC, MPC with integrator and ARMPC based on the nominal model.

2) Dynamic Performance

Then, the dynamic comparisons among MPC, MPC with integrator and ARMPC are conducted for the cases of input voltage change from 165 V to 180 V and 165 V to 195 V, resistance of the *RL* load change from 100 Ω to 80 Ω and 100 Ω to 120 Ω. The results are shown in Fig. 12. Apparently, ARMPC only takes a slightly longer time (≤1.8 ms) to the steady state than the conventional MPC. Besides, ARMPC

owns better dynamic performance than the MPC with integrator for the input voltage change.

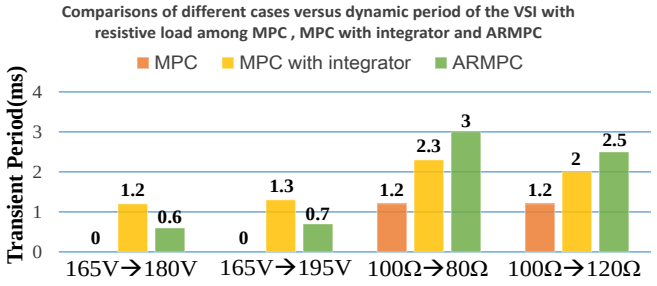

Fig. 12. Comparative bar-charts of different cases versus transient period between the VSI with *RL* load controlled by MPC, ARMPC and MPC with integrator.

V. Conclusions

Conventional finite-control-set model predictive control (FCS-MPC) will induce non-ignorable steady-state errors of the outputs when model mismatch occurs on power electronics systems. In this paper, an adaptive reference model predictive control (ARMPC) that is built upon the framework of MPC and trajectory-based control theory is proposed and experimentally verified to significantly alleviate the steady-state errors. ARMPC contains two major components. One is the virtual references that substitute the actual references to be tracked. The other one is the virtual multiple input multiple output (MIMO) system that generates required virtual references based on the past measured data. ARMPC can be easily implemented using a low-cost digital controller. As an example, ARMPC is applied on a single-phase full-bridge voltage source inverter (VSI) with both resistive and resistive-inductive (*RL*) load. The results show that ARMPC gives a better steady-state performance than the MPC when there exists a model mismatch, load change, and input voltage change. Besides, ARMPC requires no additional tuning of its control coefficients and operates efficiently over a wider operating range as compared to the MPC with integrator. The dynamic performance of ARMPC is also attractive, since less than 2 ms addition of the transient period are taken by ARMPC than the conventional MPC for the VSI with both resistive and *RL* load.

VI. Acknowledgement

The authors would like to thank the theme-based research project 23-701/14-N and the anonymous reviewers for their feedback and suggestions.

References

[1] B. K. Bose, "Energy, environment, and advances in power electronics," *IEEE Tran. Power Electron.*, vol. 15, no. 4, pp. 688–701, Jul. 2000.
[2] N. Mohan, T. M. Undeland, and W. P. Robbins, *Power Electronics*, 3rd ed. John Wiley & Sons, Inc., 2003.
[3] M. P. Kazmierkowski, R. Krishnam, and F. Blaabjerg, *Control in Power Electronics*, Academic Press, 2002.
[4] E. F. Camacho and C. Bordons, *Model Predictive Control*, Springer, 1999.
[5] J. B. Rawlings and D. Q. Mayne, *Model Predictive Control: Theory and Design*, Nob Hill Publishing, 2009.
[6] C. Garcia, D. Prett, and M. Morari, "Model predictive control: theory and practice – a survey," *Automatica*, vol. 25, no. 3, pp. 335–348, May 1989.
[7] T. Geyer, G. Papafotiou, R. Frasca, and M. Morari, "Constrained optimal control of the step-down dc–dc converter," *IEEE Tran. Ind. Electron.*, vol. 23, no. 5, pp. 2454–2464, Sept. 2008.
[8] J. M. Espi, J. Castello, and R. Garcia-Gil, "An adaptive robust predictive current control for three-phase grid-connected inverters," *IEEE Tran. Ind. Electron.*, vol. 58, no. 8, pp. 3537–3546, Aug. 2011.
[9] R. P. Aquilera, P. Lezana, and D. E. Quevedo, "Finite-control-set model predicitve control with improved steady-state performance," *IEEE Tran. Ind. Informat.*, vol. 9, no. 2, pp. 658–667, May 2013.
[10] J. Rodr ́guez and P. Cort és, *Predictive Control of Power Converters and Electrical Drives*, NJ: Wiley, 2012.
[11] K. Low, "A digital control technique for a single-phase pwm inverter," *IEEE Tran. Ind. Electron.*, vol. 45, no. 4, pp. 672–674, Aug. 1998.
[12] J. Rodriguez, M. P. Kazmierkowski, J. R. Espinoza et al., "State of the art of finite control set model predictive control in power electronics," *IEEE Tran. Ind. Informat.*, vol. 9, no. 2, pp. 1003–1016, May 2013.
[13] P. T. Krein, *Elements of Power Electronics*, Oxford Press, 1998.
[14] R. A. Decarlo, S. H. Zak, and G. P. Matthews, "Variable structure control of nonlinear multivariable systems: a tutorial," *Proc. IEEE*, vol. 76, no. 3, pp. 212–232, Mar. 1988.
[15] Y. C. Chiu, K. S. Leung, and H. S. Chung, "High-order switching surface in boundary control of inverters," *IEEE Trans. Power Electron.*, vol. 22, no. 5, pp. 1753–1765, Sept. 2007.
[16] K. W. Chan, H. S. Chung, and S. Y. R. Hui, "A generalized theory of boundary control for a single-phase multilevel inverter using second-order switching surface," *IEEE Trans. Power Electron.*, vol. 24, no. 10, pp. 2298–2313, Oct. 2009.
[17] R. Alzola, P. Kslazek, M. Ordonez, and F. Blaabjerg, "Introducing state-trajectory control for the synchronous interleaved boost converter," in *Applied Power Electron. Confer. Expo. (APEC)*, 2015, pp. 616–621.
[18] M. Ordonez, M. T. Iqbal, and J. E. Quaicoe, "Selection of a curved switching surface for buck converters," *IEEE Trans. Power Electron.*, vol. 21, no. 4, pp. 1148–1153, Jul. 2006.
[19] V. I. Utkin, *Sliding Modes in Control and Optimization*, Springer, 1992.
[20] R. Munzert and P. T. Krein, "Issues in boundary control," in *IEEE PESC*, vol. 1, pp. 810–816, Jun. 1996.
[21] S. C. Tan, Y. M. Lai, and C. K. Tse, *Sliding Mode Control of Switching Power Converters – Techniques and Implementation*, CRC, 2012.
[22] Y. Yang, S. C. Tan, S. Y. R. Hui, "Adaptive reference model predictive control for power electronics," in *IEEE Applied Power Electron. Confer. Expo.*, 2016, pp. 1169–1175.
[23] T. Kailath, *Linear Systems*, N. J.: EngleWood Cliffs, 1980.
[24] J. Rodriguez, J. Pontt, C. A. Silva et al., "Predictive current control of a voltage source inverter," *IEEE Tran. Ind. Electron.*, vol. 54, no. 1, pp. 495–503, Feb. 2007.
[25] R. Vargas, P. Cortés, U. Ammann et al., "Predictive control of a three-phase neutral-point-clamped inverter," *IEEE Tran. Ind. Electron.*, vol. 54, no. 5, pp. 2697–2705, Oct. 2007.
[26] R. Vargas, J. Rodríguez, and P. Wheeler, "Predictive current control of an induction machine fed by a matrix converter with reactive power control," *IEEE Tran. Ind. Electron.*, vol. 55, no. 12, pp. 4362–4371, Dec. 2008.
[27] P. Cortés, J. Rodríguez, D. E. Quevedo, and C. Silva, "Predictive current control strategy with imposed load current spectrum," *IEEE Tran. Power Electron.*, vol. 23, no. 2, pp. 612–618, Mar. 2008.
[28] P. Cortés, G. Ortiz, J. I. Yuz et al., "Model predictive control of an inverter with output LC filter for UPS applications," *IEEE Tran. Ind. Electron.*, vol. 56, no. 6, pp. 1875–1883, Jun. 2009.
[29] H. Abu-Rub, J. Guziniski, Z. Krzeminski, and H. Toliyat, "Predictive current control of voltage-source inverters," *IEEE Trans. Ind. Electron.*, vol. 51, no. 3, pp. 585–593, Jun. 2004.
[30] "C2000 solar DC/AC single phase inverter schematic," *http://www.ti.com/lit/df/tidr753/tidr753.pdf*, TI, 17 Jun. 2014.